AD-A235 019

‖‖‖‖‖‖‖‖‖‖‖‖‖

ΓATION PAGE

DATE	3. REPORT TYPE AND DATES COVERED
	FINAL 11 Dec 87 TO 31 Aug 90

4. TITLE AND SUBTITLE

Luminescence and Lasing in II-VI Semiconductors

5. FUNDING NUMBERS

ARPA ORDER NO 9520

6. AUTHOR(S)

Dr August Witt

7. PERFORMING ORGANIZATION NAME(S) AND ADDRESS(ES)

Massachusetts Inst of Tech
Materials Science & Engineering
Cambridge, MA 02139

8. PERFORMING ORGANIZATION REPORT NUMBER

9. SPONSORING/MONITORING AGENCY NAME(S) AND ADDRESS(ES)

AFOSR/NE
Bldg 410
Bolling AFB Washington DC 20332-6448
Dr. Gerald Witt

10. SPONSORING/MONITORING AGENCY REPORT NUMBER

F49620-88-C-0035

11. SUPPLEMENTARY NOTES

12a. DISTRIBUTION/AVAILABILITY STATEMENT

APPROVED FOR PUBLIC RELEASE: DISTRIBUTION IS UNLIMITED

12b. DISTRIBUTION CODE

13. ABSTRACT (Maximum 200 words)

The objective of this contract was to develop a method for growth of bulk semiconducting material, suitable for monolitic infrared focal plane detectors, light emitting diodes, and laser structures. The projected focused on narrow band gap HgMnTe alloys, semimagnetic semiconductors. HgMnTe is an infrared detector material with properties similar to those of HgCdTe (1,2). In particular, as our work has shown (3,4), HgMnTe electroluminesces more efficiently than HgCdTe, and p-type HgMnTe has higher conductivity than comparable p-HgCdTe; both features are advantageous in device applications.

14. SUBJECT TERMS

15. NUMBER OF PAGES

16. PRICE CODE

17. SECURITY CLASSIFICATION OF REPORT	18. SECURITY CLASSIFICATION OF THIS PAGE	19. SECURITY CLASSIFICATION OF ABSTRACT	20. LIMITATION OF ABSTRACT
UNCLASSIFIED	UNCLASSIFIED	UNCLASSIFIED	UNLIMITED

LUMINESCENCE AND LASING IN
II-VI SEMICONDUCTORS
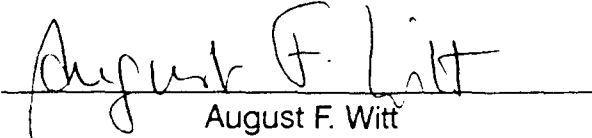
Final Technical Report

Sponsored by

H-1

Defense Advanced Research Projects Agency

Dr. James Murphy
202/694-3145

12/11/87 – 08/31/90
$356,787.54

Monitored by AFOSR under Contract No. F49620-88-C-0035

_____
August F. Witt
Principal Investigator
617/253-5303

The views and conclusions contained in this document
are those of the authors and should not be interpreted
as necessarily representing the official policies or endorsements,
either expressed or implied, of the Defense Advanced
Research Projects Agency or the U.S. Government.

LUMINESCENCE AND LASING IN
II-VI SEMICONDUCTORS

This report covers the work on Contract No. F49620-88-C-0035, DEF from November 1987 through August 1990.

1. Summary

The objective of this contract was to develop a method for growth of bulk semiconducting material, suitable for monolitic infrared focal plane detectors, light emitting diodes, and laser structures.

The project focused on narrow band gap HgMnTe alloys, semimagnetic semiconductors. HgMnTe is an infrared detector material with properties similar to those of HgCdTe (1,2). In particular, as our work has shown (3,4), HgMnTe electroluminesces more efficiently than HgCdTe, and p-type HgMnTe has higher conductivity than comparable p-HgCdTe; both features are advantageous in device applications.

During the period of this contract the research program was aimed along the following directions: (a) study of the effectiveness of axial magnetic fields for stabilization of HgMnTe melt and solutions during vertical Bridgman growth; and (b) comprehensive characterization of grown materials related to the use of these compounds for detector and laser structures.

Specific problems targeted during this investigation period included:

1. Control of the morphology of the crystal–melt interface during growth

    of HgMnTe in magnetic and non–magnetic Bridgman configuration.

2. Numerical modeling of crystal growth in magnetic and no–magnetic

    Bridgman configuration.

3. Evaluation of the crystallographic and electronic properties of HgMnTe

    alloys by fabrication and testing of the infrared detectors and

    electroluminescence devices.

4. Investigation of physical properties of HgMnTe by electrical,,

    magneto–optic and nonlinear optic experiments.

The results of this investigation have been reported at DARPA Annual Review

Meetings, international conferences, and in the open literature:

a. Publications:

1. S.Y. Yuen, P.A. Wolff, and P. Becla, "Free–Carrier Spin–Induced Faraday Rotation in HgCdTe and HgMnTe", J. Vac. Sci. Technol. A5 (5) 3040 (1987).

2. P. Becla, "HgMnTe Light Emitting Diods and Laser Heterostructures", J. Vac. Sci. Technol. A6 (4) 2725 (1988).

3. P. Becla, "Semimagnetic Semiconductor Laser", United States Patent, Patent No. 4,813,049, March 14, 1989.

4. J.B. Choi, R. Mani, H.D. Drew, and P. Becla, "Resonant Acceptor Bound Magnetic Polarous in $Hg_{0.93}Mn_{0.07}Te$", Semicond. Sci. Technol. 5, S284 (1989).

5. P. Becla, N. Grudzien, and J. Piotrowski, "Uncooled 10.6 µm Mercury Manganese Telluride Photoelectromagnetic IR Detectors", J. Vac. Sci. Technol., in press (1991).

b. Conferences and Reports

1. P. Becla and A.F. Witt, "Luminescence and Lasing in II–VI Semiconductors", DARPA Focal Plane Array Materials and Processing, Annual DARPA Meeting, Arlington, VA April 1987.

2. S. Wong, P.A. Wolff, S. Foner, and P. Becla, "The Magnetoresistance of HgMnTe in Pulsed Fields up to 45 Tesla", Meeting of the American Physical Society, St. Louis, MO, March 1988.

3. J.B. Choi, R. Mani, H.D. Drow, and P. Becla, "Hole Spin Resonance in HgMnTe: Strong Temperature Dependence of Spin Exchange", Meeting of the American Physical Society, St. Louis, MO, March 1988.

4. P. Becla and A.F. Witt, "Bulk Growth of Hg-Based Alloys and Their Applications", DARPA IR Focal Plane Arrys Materials and Processing, Annual DARPA Meeting, Arlington, VA, April 1988.

5. P. Becla, S. Motakef, A.F. Witt, J.M. Wrobel, and J.J. Dubowski, "The Effectiveness of Axial Magnetic Fields on HgMnTe Melt Stabilization During Vertical Bridgman Growth", Third Eastern Regional Conference on Crystal Growth, Atlantic City, NJ, October 18–20, 1989.

6. P. Becla, J.C. Man, and S. Motakef, "Magnetic Field Growth of HgMnTe Alloys by the Vertical Bridgman Technique", Eighth American Conference on Crystal Growth, Vail, CO, July 15–20, 1990.

7. S. Motakef, P. Becla, and J.C. Han, "Experimental and Modeling Results on the Influence of Applied Magnetic Fields on Compositional Uniformity of Directionally Solidified Semiconductors", XII ICHMT International Symposium on Heat and Mass Transfer in Manufacturing Technologies, Dubrovnik, Yugoslavia, Aug. 27–30, 1990.

2. Growth of HgMnTe Alloys in High Magnetic Field

The goal of this study was to investigate the effectiveness of axial magnetic fields on HgMnTe melt stabilization during vertical Bridgman growth. Our particular interest was to achieve uni-directional solidification at a relatively high growth rate. The effects of liquid phase composition, thermal configuration of heat transfer, the growth rate, and the magnitude of the applied magnetic field on both radial and axial compositional variation were investigated. The research program consisted of experimental and numerical modeling components.

2.1 Crystal growth experiments

The experimental part of the program focused primarily on crystal growth of HgMnTe alloys by the vertical Bridgman technique in magnetic and non-magnetic field environments and on comprehensive characterizations of the grown material. The vertical Bridgman-type growth system with axial magnetic field application is schematically illustrated in fig. 1. The growth system consists of a two-zone furnace and the superconducting magnet. A sodium heat pipe was used to obtain isothermal conditions in the hot zone and an aluminum cylinder in the cold zone acted as a heat leveler. The hot and cold zones were separated by an adiabatic zone with a temperature gradient of about 50°C/cm. A water cooled shield was installed to prevent overheating of the magnet cavity and to increase the linearity of the temperature gradient in the adiabatic zone (fig. 2). The furnace was placed inside the 12-inch commercial superconducting magnet, capable of generating axial magnetic fields of up

4

to 3 Tesla; temperature control and data acquisition was accomplished through an MBM (PC) computer. The charges were 16 mm and 22 mm in diameter and the starting melt composition was 11 and 15 mole % of MnTe in HgTe. The temperature gradient in the adiabatic zone was kept constant at about 50°C/cm, and the growth rate (charge displacement rate) ranged from 0.8 mm/hr to 1.2 mm/hr.

The ingots were sliced longitudinally and perpendicular to the growth direction. Microprobe analysis, electroreflectivity, and optical transmission measurements were used to map compositional variations.

Figures 3 and 4 present typical graphs of the axial and radial compositional diagrams of HgMnTe ingots grown in our Bridgman facility. As the overall electro-optical quality of this material is largely controlled by the uniformity in Mn concentration, figs. 3 and 4 reflect the state-of-the-art for growth of HgMnTe to be used in device applications. The axial and radial composition of a crystal grown in the presence of an applied axial magnetic field ($\beta = 3$ Tesla) is shown in fig. 5. The results indicate that during growth in the presence of an axial magnetic field the resulting material is axially and radially much more uniform in composition than in the absence of a magnetic field. During growth without a magnetic field, crystal composition reflects convective interference with segregation similar to results shown in fig. 4. A comparison of the detailed structure of radial composition in conventional and magnetically grown materials, obtained by electro-reflectivity measurements, is shown

in fig. 6. Results reveal the presence of a fine non-uniform microsegregation structure in the conventionally grown material which is not observed for growth from magnetically stabilized melts.

Our experimental results demonstrate the effectiveness of magnetic fields on Mn composition control of Hg-based ternary compounds. Further improvements in composition control are expected to be achieved only in a microgravity environment. We anticipate our findings to have substantial impact on crystal growth and related device technology.

2.2 Numerical modeling of crystal growth

The interference of buoyancy-driven convection with segregation at the growth interface is the primary cause of axial and radial compositional nonuniformity of the grown material. We have analyzed this issue for lightly-doped materials. The results have been presented at two international conferences and have been submitted for publication in the Journal of Crystal Growth.

During growth of HgMnTe the lighter component, MnTe, is preferentially incorporated into the solid, resulting in an effective rejection of the heavier Hg-based component. This sets up very strong "solutal" forces which are stabilizing in the axial direction. A typical velocity profile driven by the radial temperature gradient close to the solidification front and the solute rejection at the growth interface is schematically shown in fig. 7. As the solute is rejected into the melt, the region close to the growth front

becomes denser and the circulating convective cell is pushed upwards, away from the growth interface.

Of interest is the appearance of a set of (weak) axially circulating cells in the zone close to the growth front. We believe the fine radial microsegregation structure shown in fig. 6 is related to the presence of these cells in our growth system. An axial plot of the difference in the species concentration at the two vertical walls ($\Delta\phi$) for non-magnetic and magnetic simulation is shown in fig. 8. The plot corresponding to the non-magnetic case clearly indicates lateral non-uniformities in the solute field which are reflected in the experimental results shown in fig. 6. Fig. 8 also shows the elimination of solute non-uniformities in the presence of a magnetic field.

The modeling results are consistent with the experimental observations, and provide a clear picture of phenomena controlling compositional uniformity in II-VI compounds grown from the melt.

3. IR Detectors Utilizing HgMnTe Alloys

The electronic properties of HgMnTe alloys have been analyzed and used for fabrication of IR photovoltaic (PV) and photoelectromagnetic (PEM) detectors.

Samples were characterized on a routine basis via: (a) IR absorption near the Γ point; (b) electroreflectivity near X and '. point; (c) microprobe analysis; and (d) transport measurements. As-grown HgMnTe samples were always p-type. due to Hg vacancies, with N_A-N_D in the range of (3-8) x 10^{17}/cc. After annealing, the material becomes n-type with n ~ 5 x 10^{14} to 10^{15}/cc. Electron mobilities (at 77K) for x $\simeq$ 0.11 are in the 10^5-10^6 cm^2/Vs range.

IR absorption spectra for the as-grown and annealed samples are shown in fig. 9. Pronounced absorption in the as-grown p-type samples is due to a high concentration of mercury vacancies which act as heavy holes. After annealing the absorption coefficient is significantly reduced.

p-n junctions were made by annealing p-type samples cut from as-grown material in a Hg saturated atmosphere. The time, the annealing temperature, and the method of producing the p-n structures have been discussed in our publications (5,6). HgMnTe homojunctions exhibit good I-V characteristics at 77K; they are superior to those made in HgCdTe crystals (2). By controlling the Mn content, the peak photoresponse of these detectors could be varied from 1.6 μm to 12 μm. Typical spectral characteristics of photovoltaic HgMnTe detectors are shown in fig. 10. The

sensitivity and detectivity of HgMnTe detectors compares favorably with those of good quality HgCdTe. The measured detectivities of 1.05×10^{11} and 3.6×10^{10} cm $Hz^{1/2}w^{-1}$ for detectors with a photoresponse peak of 5.3 μm and 10.6 μm, respectively, are close to the background limit.

Considerable effort has been made in the formation of uncooled 10.6 μm HgMnTe PEM detectors (7). We performed numerical and experimental analyses of the PEM effect utilizing HgMnTe material. The normalized responsivity, R_V, detectivity, D^*, and time constant, τ, were calculated using Lile's generalized theory of the PEM effect (8). A responsivity (R_V) of 0.1 V/w and a detectivity (D^*) of 1.2×10^7 cm $Hz^{1/2}w^{-1}$ were achieved with p-type $Hg_{1-x}Mn_xTe$ of composition x ~ 0.08 and an acceptor concentration N_o ~ 10^{17} cm^{-3}. The experimental values of R_V and D^* were very close to the calculated values. The main advantage of HgMnTe PEM detectors is their very low noise (N_V) and wide frequency bandwidth (the frequency characteristics are flat over the frequency region, starting from CW to several GHz).

4. HgMnTe Light Emitting Diodes and Laser Heterostructures

HgMnTe p-n junctions electroluminesce moderately efficiently in the temperature range from 10K to 200K. Internal efficiency at the wavelength range 5.3 μm has been recorded to be in the range of a few %. Double n-p-p$^+$ laser heterojunction structures were fabricated by a combination of Bridgman, isothermal vapor, and liquid phase epitaxy growth, substitutional doping, and annealing in a mercury saturated atmosphere (3,4). A schematic of the double heterojunction HgMnTe laser structure is presented schematically in fig. 11. Simulated emission has been achieved at the wavelength (λ) of 5.3 μm at 77K using pulsed current of about 1.3 kA/cm^2. The half-width of the peak was in the range of ~1.5 x 10^{-3} μm.

In the low temperature region (5-10K) the electrical and optical characteristics are found to improve when external magnetic fields are applied. High and positive magnetic tuning was also achieved. This new effect (associated with huge spin splitting in HgMnTe) suggests the feasibility of achieving magnetically tunable lasers. More work is needed, however, to optimize doping, reduce the internal resistivity, and increase the stability of HgMnTe devices.

5. Physical Properties of HgMnTe

5.1 Free-carrier spin-induced Faraday rotation in HgCdTe and HgMnTe

We have examined the free-carrier, spin-induced Faraday rotation in n-type HgCdTe and HgMnTe in the 10.6 μm region (9).

At low laser intensities, similar results were obtained in $Hg_{0.78}Cd_{0.22}Te$ and $Hg_{0.89}Mn_{0.11}Te$, although in general the Verolet constant of HgMnTe was higher for the same doping level, probably because of the higher effective g-value. As the laser intensity on HgCdTe is raised, the saturation level increases. In HgMnTe the linear Faraday rotation is found to decrease as the emission intensity increases. These phenomena can be explained by the spin-heating effect: the Faraday rotation is reduced if the electron spins are depolarized due to thermal agitation. In HgCdTe, the laser raises the electronic translational energy, but the electron spin remains cold since spin-flip scattering processes are infrequent. In semimagnetic semiconductors, however, the carrier spin and translation energies are rapidly equilibrated via the carrier-Mn^{2+} exchange interaction, elevating the spin temperature. The laser-induced polarization also prevents the spin from being fully aligned, thus explaining the high saturation field observed in HgMnTe under strong irradiation.

This effect may be applicable as switchable, tunable infrared filters or as insulators.

11

5.2 Resonant acceptor bound magnetic polarons in HgMnTe

Bound magnetic polarons (BMP's) have so far been extensively investigated only in wide-gap semiconductors (10,11). In the case of narrow-gap semimagnetic semiconductors, the zero-field spin splitting observed in PbMnS and PbMnTe (12) and magneto-optical transition observed in HgMnTe (13) have been controversially interpreted as possible evidence for the formation of free magnetic polarons (FMP's).

Our investigations (14) have provided evidence for a resonant acceptor bound magnetic polaron (RABMP) in zero-gap p-type semimagnetic $Hg_{1-x}Mn_xTe$ (x = 0.065 and 0.070). The magnetic field and temperature dependent resonant acceptor energy have been deduced from far-infrared magneto-optical measurements of the impurity transition between the resonant acceptor and the uppermost heavy hole state. The resulting zero-field binding energy of the resonant acceptor was observed to increase rapidly as the temperature was lowered to zero and saturated at $T \geq$ 16K. This information is very important for understanding the magneto-optical properties of semimagnetic semiconductors.

References

1. J.K. Furdina. J. Vac. Sci. Technol. 21, 220 (1982).

2. Panel discussion on technology, Proc. Conf. on Physics of Narrow Gap Semiconductors, Linz (1981), Springer-Verlag, Berlin (1982), p. 280.

3. P. Becla, J. Vac. Sci. Technol. A6, 2725 (1988).

4. P. Becla, U.S. Patent, No. 4,813,049 (1989).

5. P. Becla, J. Va. Sci. Technol. A4, 2014 (1986).

6. S. Wong and P. Becla, J. Va. Sci. Technol. A4, 2019 (1986).

7. P. Becla, N. Grudzien and J. Piotrowski, J. Vac. Sci. Technol., in press (1991).

8. D.L. Lile, Phys. Rev. B8, 4708 (1973).

9. S.Y. Yuen, P.A. Wolff, P. Becla, and D. Nelson, J. Vac. Sci. Technol. A5, 3040 (1987).

10. D. Heiman, P.A. Wolff, and J. Warnock, Phys. Rev. B27, 4849 (1983).

11. M. Bugajski, P. Becla, P.S. Wolff, D. Hieman, and L.R. Ram-Mohan, Phys. Rev. B38, 10512 (1988).

12. G. Kavsrewski and L. Kowalcryk, Solid State Commun. 48, 653 (1983).

13. R. Stepniowski, Solid State Commun. 58, 19 (1986).

14. J.B. Choi. R. Mani, H.D. Drew and P. Becla, Semicond. Sci. Technol. 5, S284 (1989).
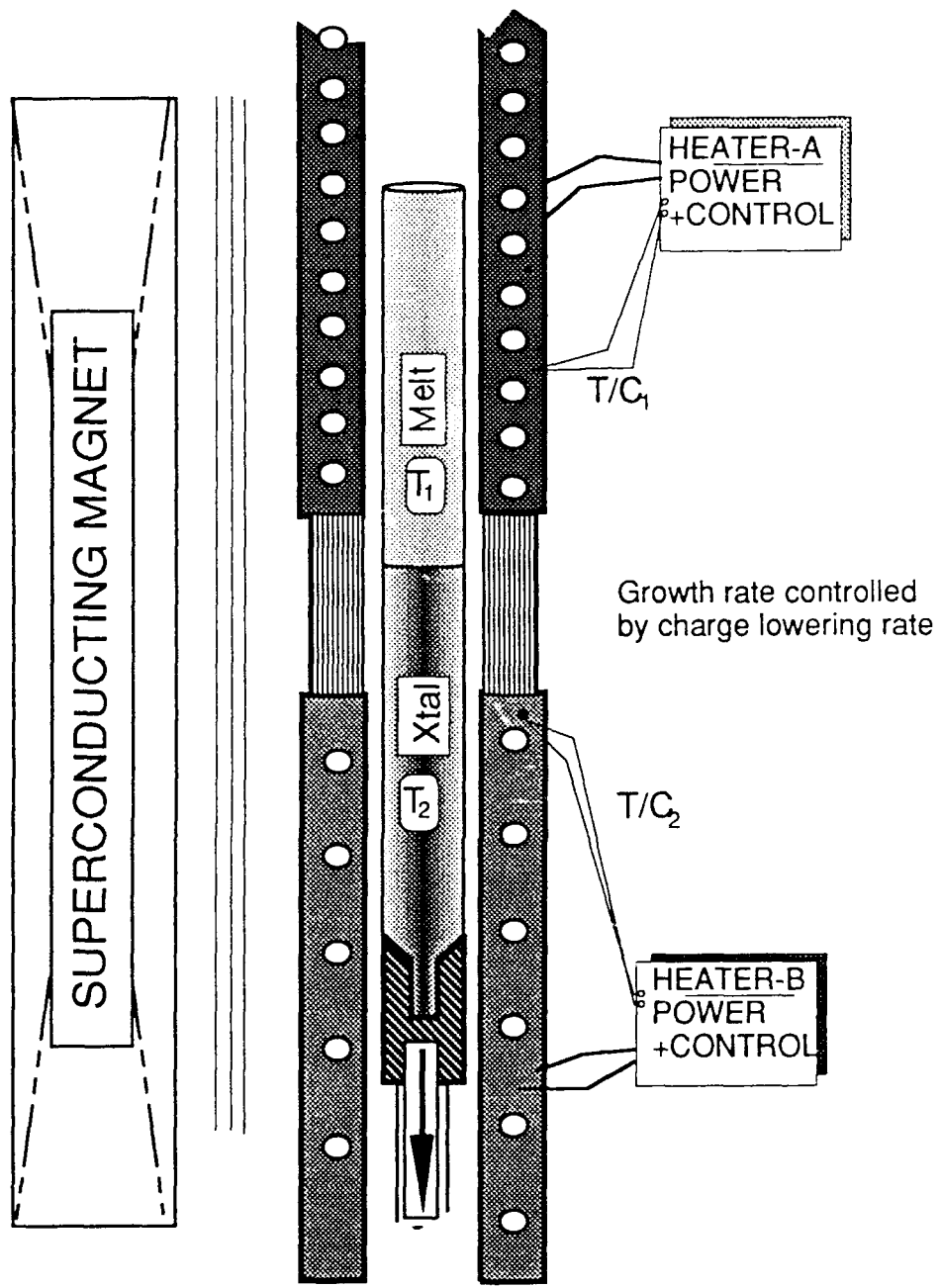
Figure Captions

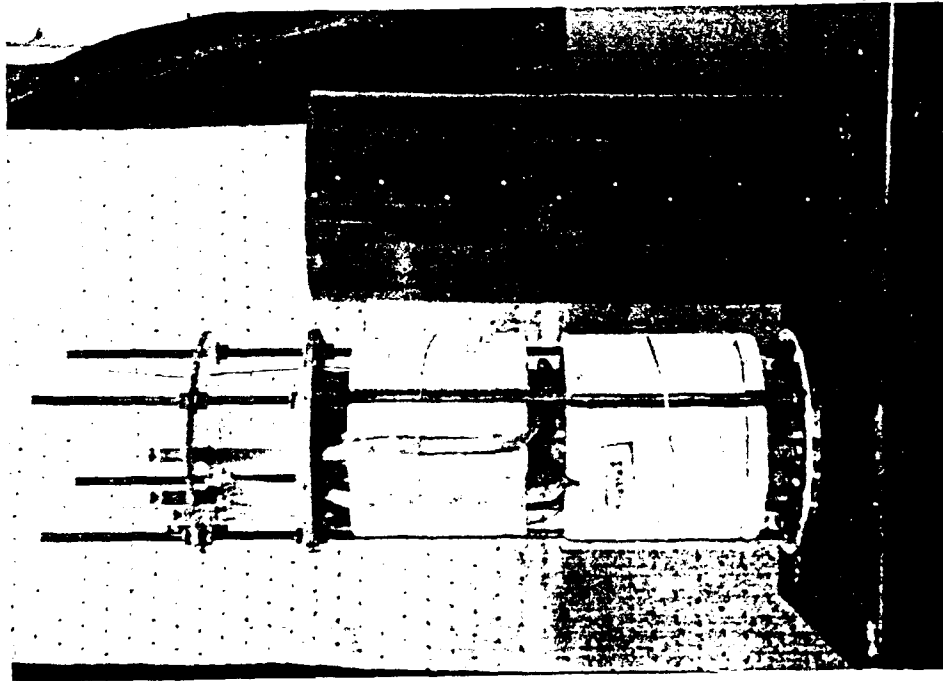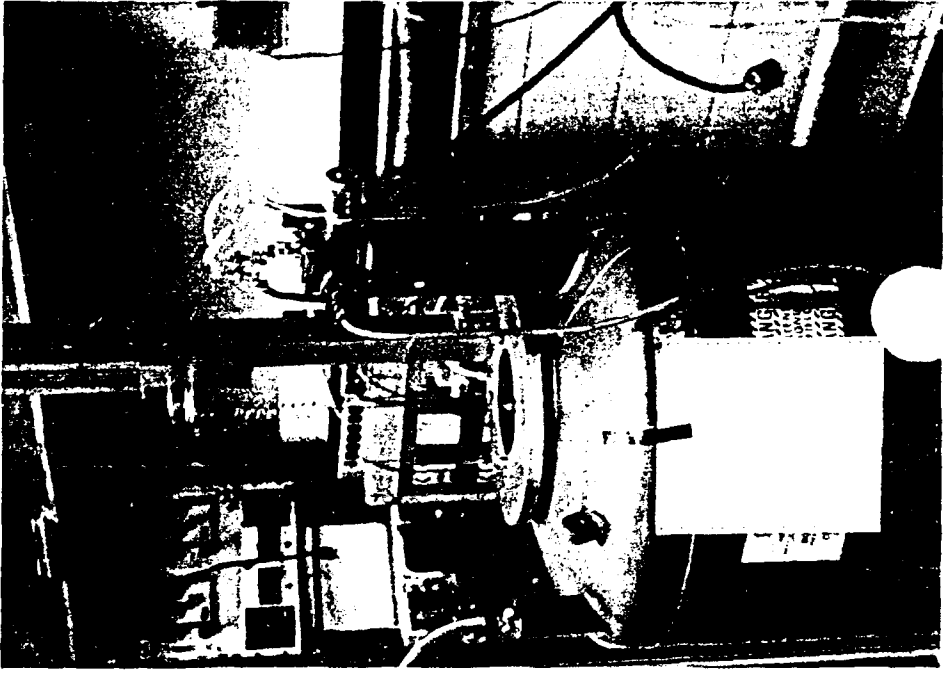Fig. 1   Schematic of the vertical magnetic Bridgman type growth system.

Fig. 2   Photograph of the magnetic Bridgman growth system. (a) Section of the
hot and cold zones; (b) general view.

Fig. 3   The axial and radial compositional uniformity in a HgMnTe ingot grown by
the vertical Bridgman technique (starting composition: x = 15%, B = 0).
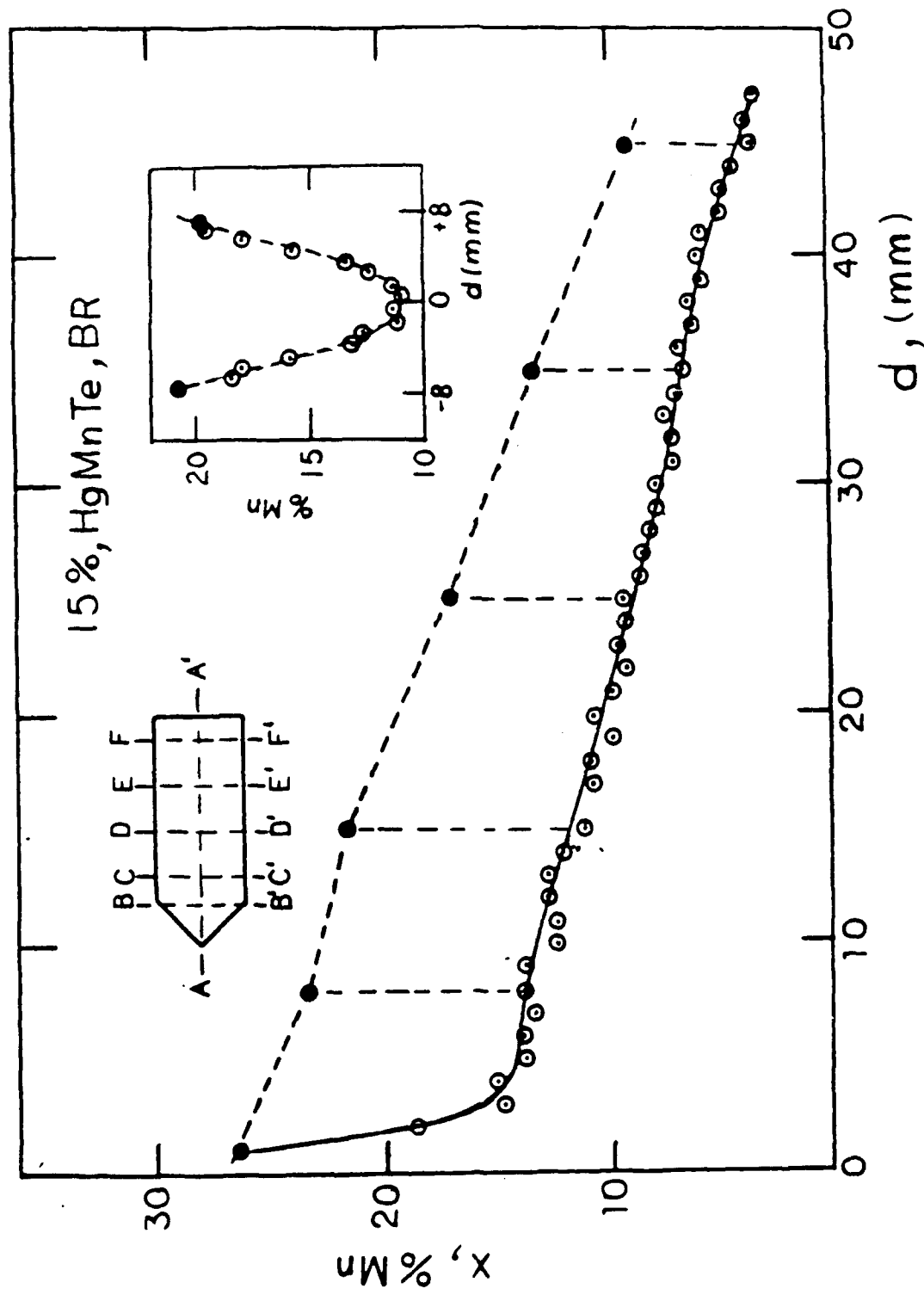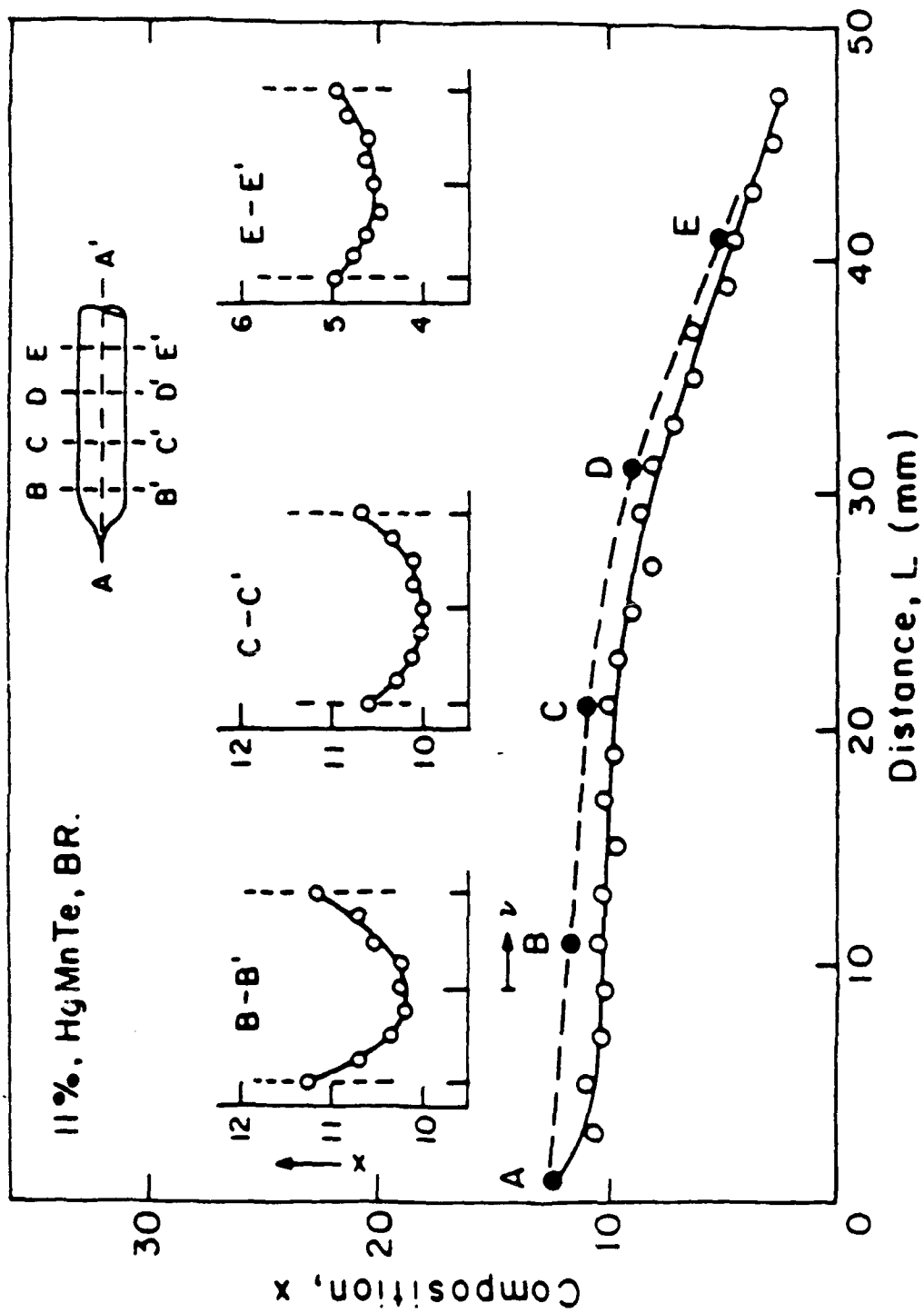
Fig. 4   The axial and radial composition uniformity in a HgMnTe ingot grown by
the vertical Bridgman technique (starting composition: x = 11%, B = 0).

Fig. 5   The axial and radial compositional uniformity in a HgMnTe ingot grown by
the vertical magnetic Bridgman technique (starting composition: x =
11%, B = 3 Tesla and 0 Tesla).
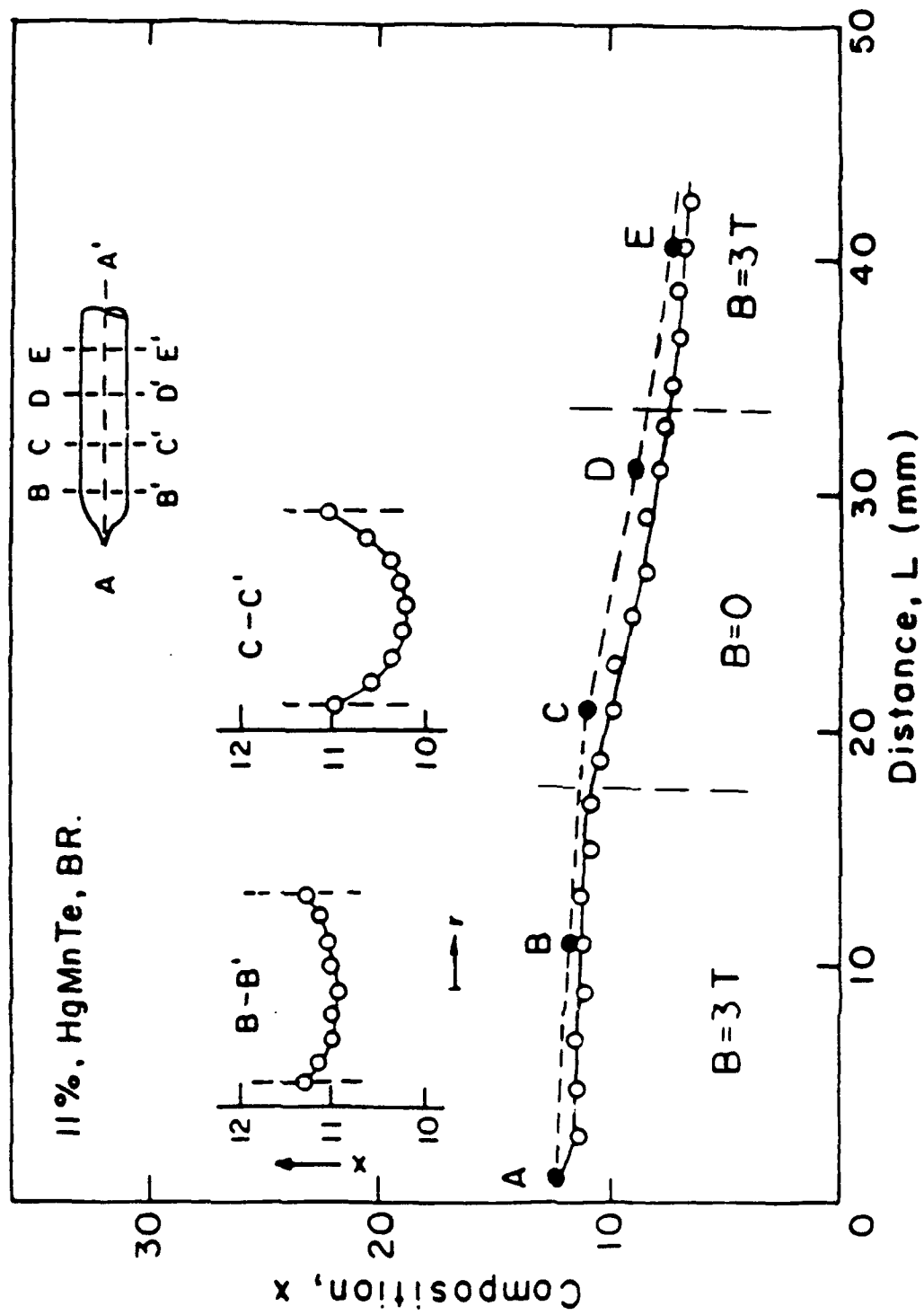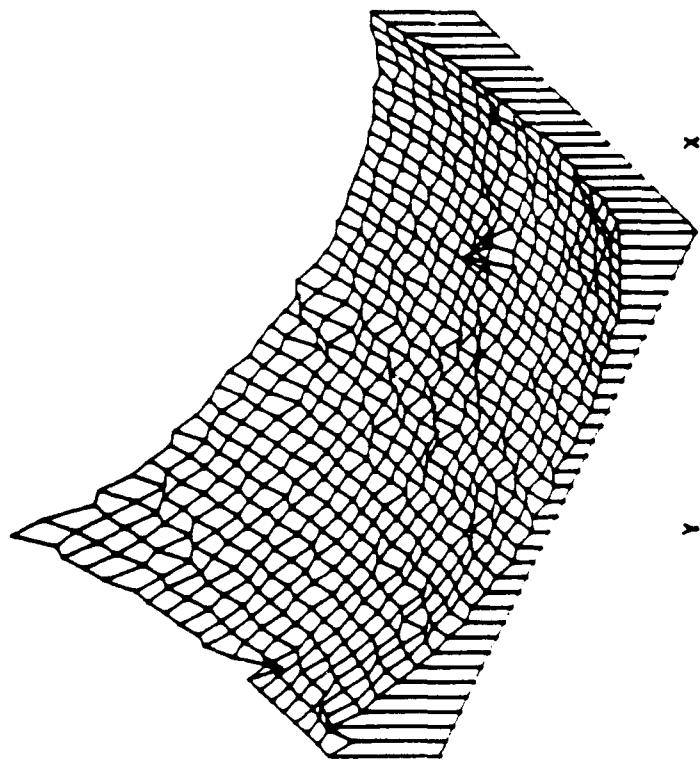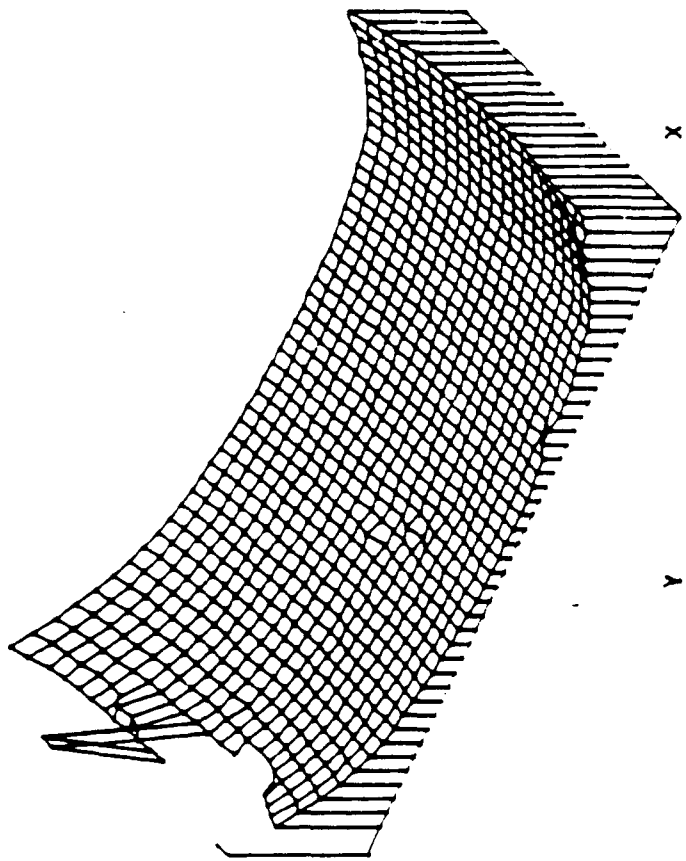
Fig. 6   Profile of $E_1 + \Delta$ transitions in a HgMnTe wafer (x ~ 11%) obtained by
electro-reflectivity measurements. Profile reflects the distribution of Mn in
a HgMnTe wafer grown by (a) conventional Bridgman, (b) magnetic
Bridgman.

Fig. 7 Convective melt flow velocity profile controlled by the radial temperature gradient close to the solidification front and by solute rejection at the growth interface.

Fig. 8 Axial plot of the difference in the species concentration at two vertical walls ($\Delta\phi$) for non-magnetic and magnetic stimulation.

Fig. 9 IR absorption spectra for as-grown and annealed HgMnTe samples.

Fig. 10 Spectral characteristics of photovoltaic HgMnTe detectors.

Fig. 11 Schematic of the double heterojunction laser structure produced in this study. (a) Geometry of the n, p and p$^+$ regions; (b) diagram of refractive index as a function of position, n; and (c) hypothetical energy band diagram for the laser structure.

SUPERCONDUCTING MAGNET

HEATER-A POWER +CONTROL

T/C₁

Melt

T₁

Growth rate controlled by charge lowering rate

Xtal

T₂

T/C₂

HEATER-B POWER +CONTROL

Fig. 1 Schematic of vertical magnetic Bridgman system used

Fig. 2   Photograph of the magnetic Bridgman growth system.   (a) Section of the

hot and cold zones; (b) general view.

Fig. 3   The axial and radial compositional uniformity in a HgMnTe ingot grown by

the vertical Bridgman technique (starting composition: x = 15%, B = 0).

Fig. 4   The axial and radial compositional uniformity in a HgMnTe ingot grown by the vertical Bridgman technique (starting composition: x = 11%, B = 0).

Fig. 5   The axial and radial compositional uniformity in a HgMnTe ingot grown by

the vertical Bridgman technique (starting composition: x = 11%, B =

3 Tesla and 0 Tesla).

RADIAL DISTRIBUTION OF Mn
Electro-reflectivity Measurement.

CONVENTIONAL
BRIDGMAN-GROWN

MAGNETIC
BRIDGMAN-GROWN

Fig. 6   Profile of $E_1 + \Delta$ transitions in a HgMnTe (x ~ 11%) wafer obtained by

electro-reflectivity measurements. Profile reflects the distribution of Mn in

a HgMnTe wafer grown by (a) conventional Bridgman, (b) magnetic

Bridgman.

SIMULATION OF TRANSIENT THERMO-SOLUTAL CONVECTION IN A CAVITY

$Gr_{TH} = 10^4$

$Gr_S = 10^7$

SOLUTE REJECTION

TIME
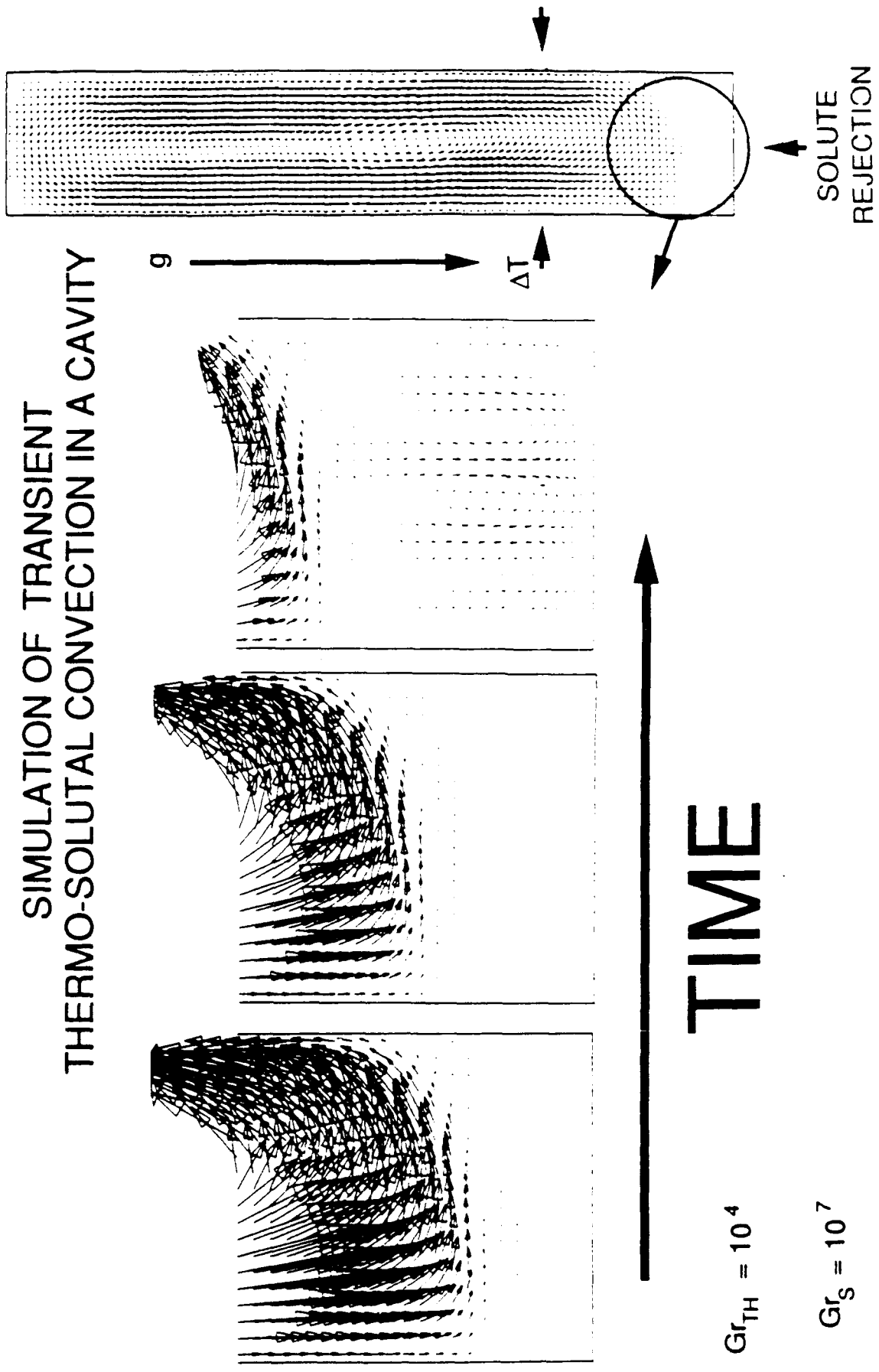
Fig. 7   The velocity profile driven by the radial temperature gradient close to the solidification front and the solute rejection at the growth interface.

SIMULATION OF TRANSIENT
THERMO-SOLUTAL CONVECTION IN A CAVITY

$Gr_{TH} = 10^4$

$Gr_S = 10^7$

MAGNETIC FIELD STRENGTH
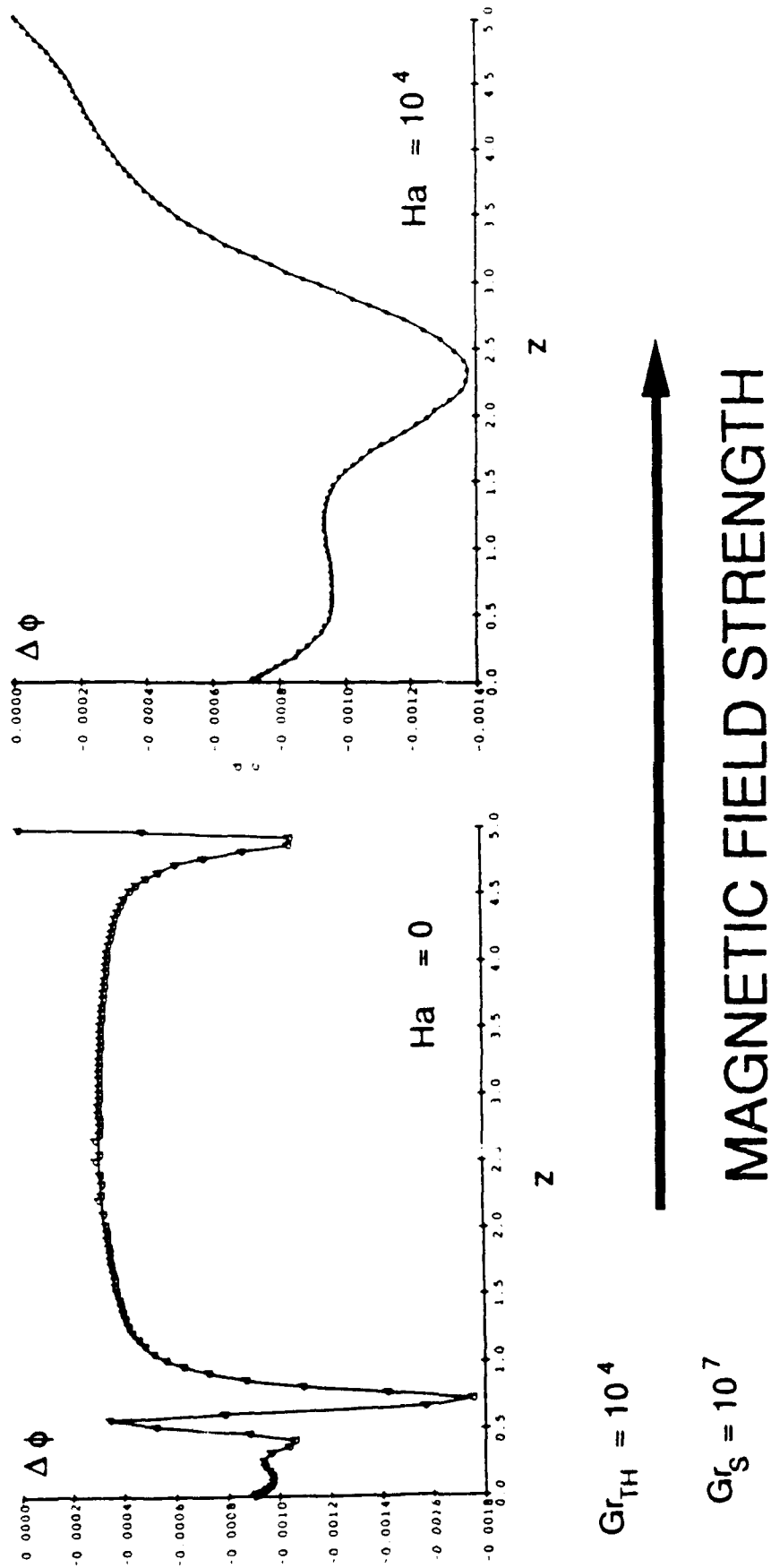
Fig. 8   An axial plot of the difference in the species concentration at two vertical

walls ($\Delta\phi$) for non-magnetic and magnetic stimulation.
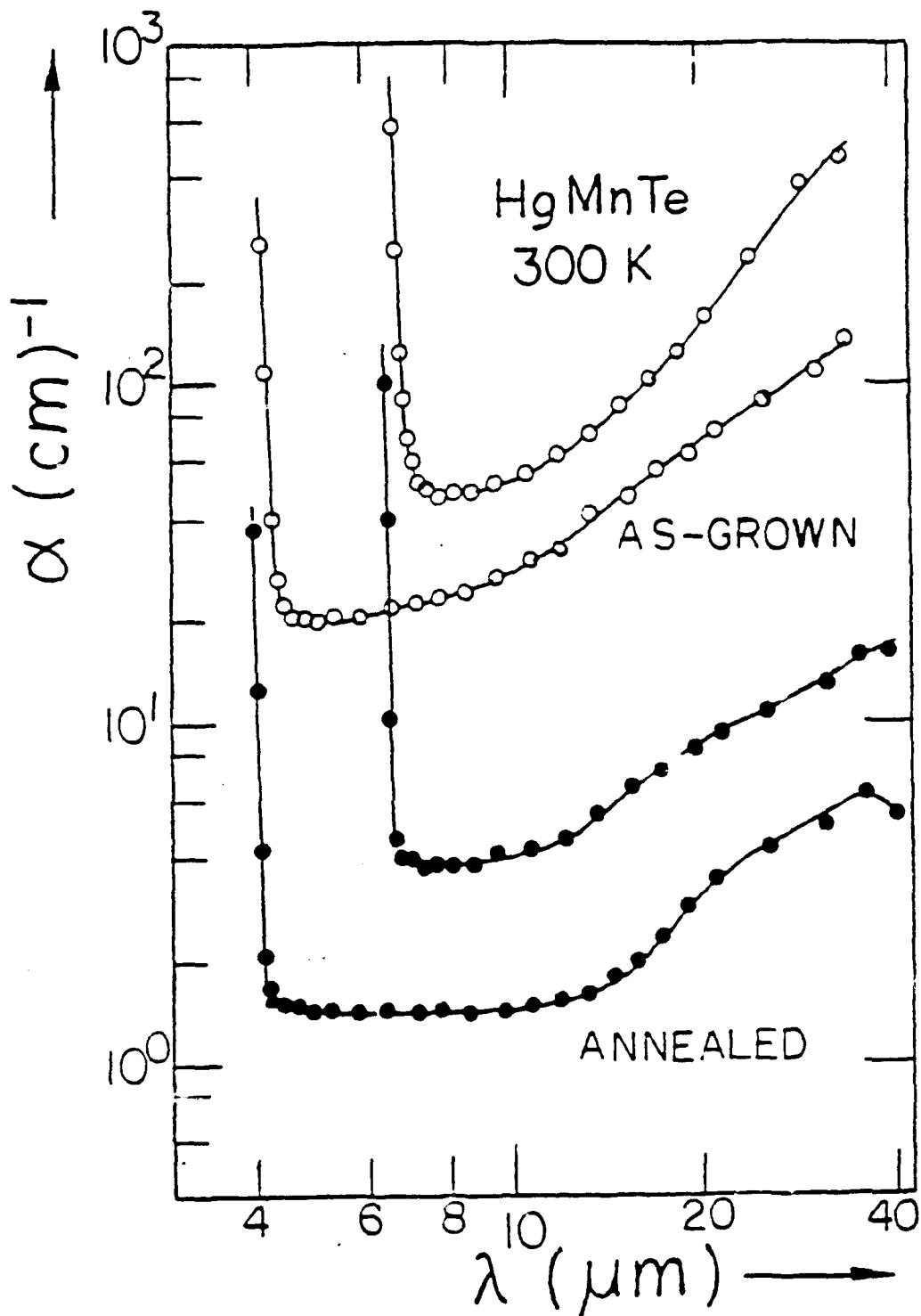
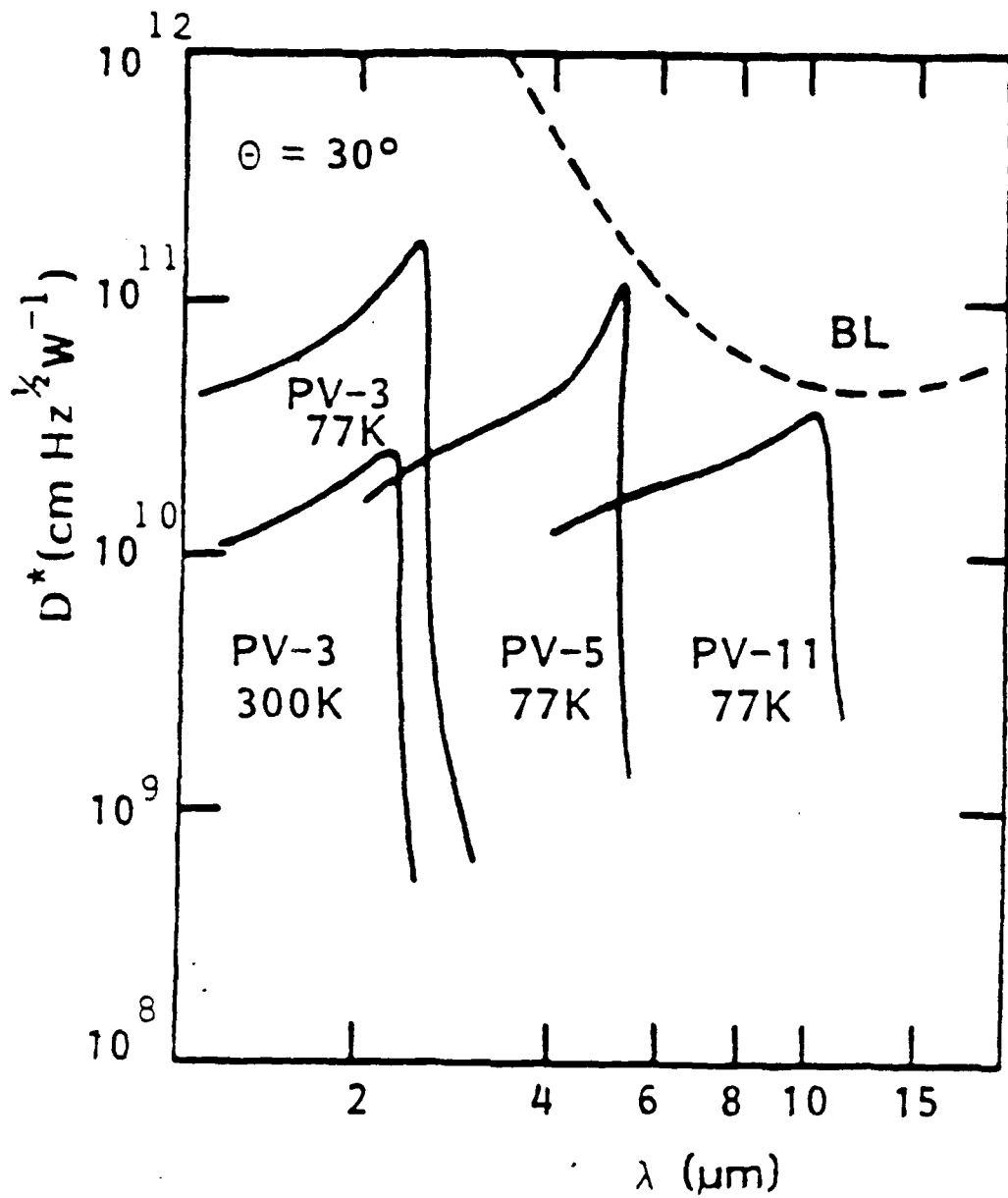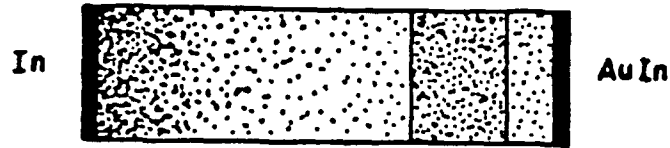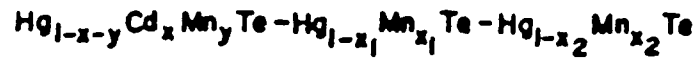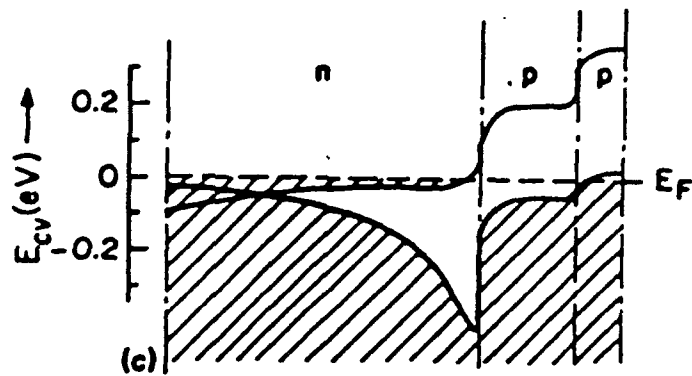Fig. 9   IR absorption spectra for the as-grown and annealed HgMnTe samples.

Fig. 10   Spectral characteristics of the photovoltaic HgMnTe detectors.

Fig. 11   Model of the double heterojunction laser structure. (a) The geometry of

the n, p and p^+ regions; (b) the diagram of the refractive index, n; and

(c) hypothetical energy band diagram.